VIBRATION ANALYSIS OF A FLEXIBLE ROTATING BEAM INCLUDING A MECHANISTIC HYSTERETIC CONTACT

RAMIN MASOUDI

Assistant Professor Department of Mechanical Engineering, American University in Dubai
E-mail: rmasoudi@aud.edu

Abstract- The dynamic and vibration behavior of a rotating flexible beam system including a nonlinear hysteretic contact is studied in this paper. Euler-Bernoulli beam theory, together with Lagrang's method is utilized to obtain the governing equations of motion for the system. The finite element method is used as the discretization procedure for the flexible cantilever beam, which can be considered a distributed parameter system. A micromechanical model for nonlinear compression hysteresis of random fiber networks was developed and examined on the felt-covered contact interfaces in the dynamic system. The obtained results confirms the efficacy of the contact model in terms of accuracy and keeping the simulation time tractable.

Keywords- Flexible Rotating Beam, Hysteretic Contact, Micromechanical Modelling, Vibration Analysis.

I. INTRODUCTION

Rotating flexible beams including contact have a wide range of engineering applications, especially in robotics. Masoudi et al. [1], [2] applied the dynamic modeling of a flexible hub-beam system including contact to design a piano key actuator. The main objective of that research was developing a device to achieve a desired finger-key contact force profile that realistically replicates that of a real pianist's finger. One of the contact interfaces in the model was covered with felt, a fiber assembly, exhibiting nonlinear hysteretic behavior in compressional loading schemes. Figure 1 shows the speed-dependent hysteresis generated by a felt-covered interface in a dynamic force-compression scheme [1]-[3].

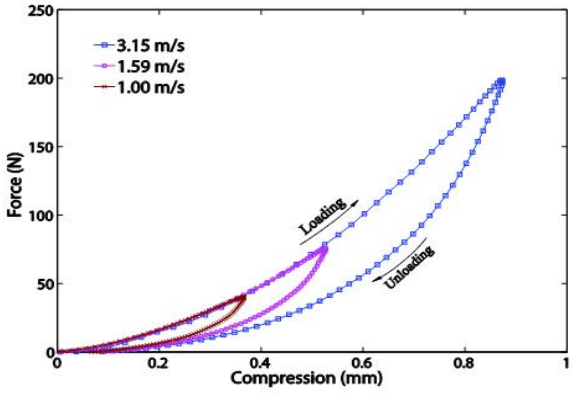


Fig.1. Loading and Unloading Curves for Dynamic Force-compression of A Felt-covered Hammer Impacting a Rigid Stop at Various Velocities.

The main issue with the proposed contact model in the actuating device was utilizing a math-based hysteretic model in which there was no physical significance for the model parameters. In this work, we propose a physics-based contact model, which improves the fidelity of the system. Moreover, it provides a context for further design analyses, e.g. sensitivity analysis and model reduction.

There are several modeling schemes to include contact phenomena in the physics-based modeling of dynamic systems, of which the regularized approach, also called continuous analysis, has shown promising performance in terms of modeling accuracy and computational efficiency. Simplistic equivalent force-deformation systems including the hysteresis effect (e.g. nonlinear spring-damper models), which relate the dynamic contact force to the relative penetration depth and rate of contacting bodies [4], [5], are among the well-known modeling schemes for this force-based approach.

In the regularized method, continuous force-deformation relations govern interaction evolution between bodies based on the compliance and damping properties of contact interfaces. Hysteresis generated by the models proposed by Gilardi and Sharf [4] and Flores et al. [5] is speed-dependent, implying viscoelastic behavior of the materials in contact. The contact problem is more complicated when the energy loss observed in the loading-unloading process is speed-independent. In this case, the source of hysteresis can be attributed to dry friction between micro-structure components of interfaces. Felt, as a nonwoven fibrous material formed by interlocked wool fibers, possesses such mechanical properties in compressive loading schemes. Masoudi et al.

[2], [3] used Scanning Electron Microscopy (SEM) to superficially analyze the fiber surface in a fiber network. According to their experimental study, the fiber seems to be rough enough to cause considerable friction between interacting fibers. For the automated key actuator, arm flexibility should reflect the overall biomechanical compliance of the pianist, including that of the fingertip pulp, as seen at the key surface in Fig. 2. Since the arm acts as a flexible beam, its characteristics can produce undesired reaction forces, especially during the contact period between the felt under the key front and the key. The problem is

analyzed here by constructing a dynamic model of the overall actuation system, including the input torque produced by the motor, the hub, flexible arm, eccentric tip mass at the end of the arm, and the contact interface between key and stop. Modeling flexible links using different dynamic criteria besides appropriate discretization methods has been noticed by many researchers in the past several decades. Actuator model realism is enhanced by including an eccentric tip mass at the end of the flexible beam. Cai et al. [7] considered a dynamic system of a rigid hub and a flexible cantilever beam with a tip mass and characterized it based on Hamilton theory and FEM. The obtained equations included axial beam extension and the second-order coupling term, i.e. the axial shrinking quantity caused by transverse displacement. Chapnik et al. [8] utilized FEM in modeling a single-link flexible robotic arm, including the effects of beam damping and also hub inertia in the dynamic equations, then simulated the motion of the arm under impact loading. The dynamics of a radially rotating beam with impact was also studied by Yigit, Ulsoy, and Scott [8], [9]. In their impact model, the vibration behavior of the system after impact was determined by the momentum balance method and a coefficient of restitution. In another paper [10] a different impact model based on Hertzian contact and damping was used to predict the rigid-body motion as well as the elastic motion of the arm during and after impact. The governing equations of motion were formulated by the extended Hamilton's principle and Euler-Bernoulli beam theory.

II. DYNAMIC MODELING OF THE KEY ACTUATOR MECHANISM

The prototype model of the finger actuator mechanism proposed by Hirschkorn et al. [11], reproducing the finger force on the key, is shown in Fig. 2. The actuation system consists of a flexible arm attached to a DC brushless rotary motor through a hub. The compliant arm behaves as a cantilever beam to which an eccentric tip mass has been attached at its free end.

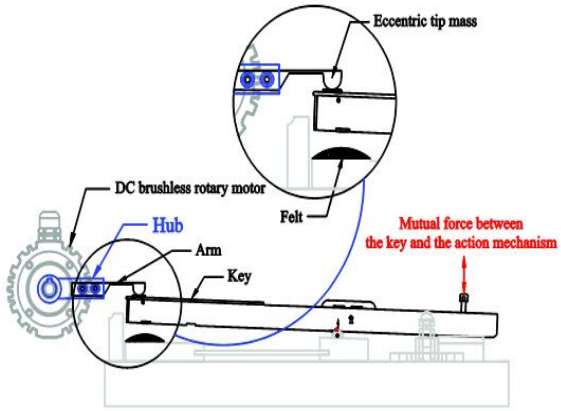


Fig.2. Key actuation system for a typical piano action mechanism.

During the piano key stroke, the contact force input from the tip causes the key to rotate and impact the ground through an interface lined with stiff felt to suppress vibrations and noise. Euler-Bernoulli beam theory along with Lagrange's method is utilized to obtain the governing equations of motion for the system. The finite element method is used as the discretization procedure for the flexible cantilever beam, representing a distributed parameter system.

To include contact dynamics at the stop, the nonlinear hysteretic behavior of felt under compression is modeled in such a way that smooth transitions between loading and unloading stages are produced, ensuring accurate response under dynamic conditions, particularly with partial loading and unloading states that occur during the contact period. The contact force model has been discussed thoroughly in the next section.

As shown in Fig. 3, the dynamic response of the piano action mechanism is replaced with the equivalent force (FFaction) on the finger tip, which will be negligible after the key touches the balance rail felt (during key-balance rail contact). FFfelt is the contact force between the key and felt underneath, which mathematically is represented by a Heaviside function in terms of penetration depth, i.e. the force is zero when there is no contact. It is important to note that the key is assumed to transfer the contact force from the felt to finger arm directly, i.e. the key and finger contact in Fig. 2 is considered to be permanent and undetachable during the simulation.

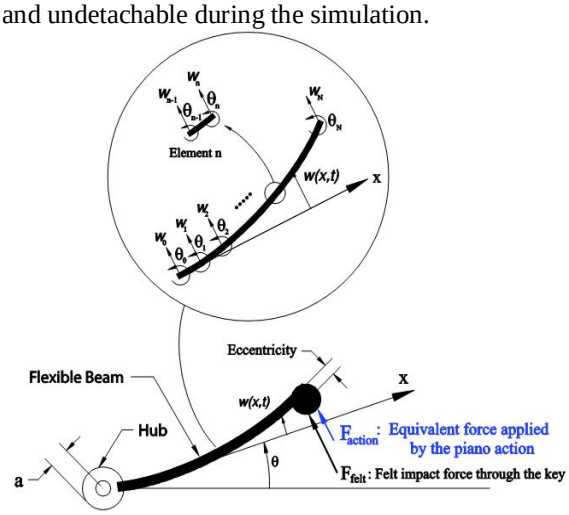


Fig.3. Schematic of the rotating flexible beam with impact, representing the simplified actuation system

As shown in Fig. 3, the actuation system consists of a rotating hub with a flexible cantilever beam fastened tightly to its free end. An eccentric tip mass has been attached to its free end in order to continuously transfer the torque applied on the hub through the arm to the key. In this work, the FEM is used as the spatial discretization procedure for the flexible beam due to its versatility and high accuracy.

To obtain the dynamic equations governing the behavior of the system, Lagrange's method is employed in which the kinetic and potential energy of

the whole system should be calculated. To apply the approach, kinetic and potential energies associated with each component of the mechanism

will be calculated and then its contribution in the overall dynamic behavior of the system is introduced into the global coefficient matrices of the dynamic equations. If we consider NN elements for the flexible beam, the generalized coordinates $\boldsymbol{qq}$ for the whole system will be

$$\boldsymbol{q}_{2N+3\times1} = \{\theta\ w_0\ \theta_0\ w_1\ \theta_1\ \dots\ w_N\ \theta_N\}^T \quad (1)$$

in which $wwnn(xx,tt)$ is the elastic displacement for the element nn, $\theta\theta nn$ and $\theta\theta nn-1$ are rotations at the end nodes, and $\theta\theta$ is the hub rotation angle (see Fig. 3). Accordingly, the kinetic energy can be written as

$$KE = \frac{1}{2}\dot{\boldsymbol{q}}^T \boldsymbol{M}\dot{\boldsymbol{q}} \quad (2)$$

and the potential energy equation will be

$$PE = \frac{1}{2}\boldsymbol{q}^T \boldsymbol{K}\boldsymbol{q} \quad (3)$$

In (2) and (3), $\boldsymbol{MM}$ and $\boldsymbol{KK}$ are respectively global mass and stiffness matrices that can be acquired by assembling local mass and stiffness matrices [2]. The generalized forces used in Lagrange's formulation are due to torque applied by the motor on the hub (TTh), the equivalent reaction force (FFaction), and the key-stop contact force which exists only when contact is detected ($HH(\varepsilon\varepsilon pp)FF$felt). ($\varepsilon\varepsilon pp$) is the Heaviside step function and $\varepsilon\varepsilon pp$ is the penetration depth of the virtual key in the felt underneath during the contact. The effect of gravity ($FFGG$) is included in generalized force because of its nonlinear relation with the generalized coordinates. Altogether, we have [1], [2]

$$\delta W_{F(t)} = \delta W_{(T_h + F_{\text{action}} + F_G + H(\varepsilon_p)F_{\text{felt}})} \quad (4)$$

The equations of motion can be obtained using Lagrange's equations in matrix form as

$$\frac{\mathrm{d}}{\mathrm{d}t}\left(\frac{\partial \mathcal{L}}{\partial \dot{\boldsymbol{q}}}\right) - \frac{\partial \mathcal{L}}{\partial \boldsymbol{q}} = \boldsymbol{Q} \quad (5)$$

in which $\mathcal{L}$ is the Lagrangian $LL=KKKK-PPPP$and $\boldsymbol{QQ}$ is the generalized force vector. Substituting kinetic and potential energy equations (2) and (3), the governing differential equations will be in the form

$$\boldsymbol{M}\ddot{\boldsymbol{q}} + \boldsymbol{K}\boldsymbol{q} = \boldsymbol{Q} \quad (6)$$

Modeling the contact force ($\varepsilon\varepsilon pp$)$FF$felt appearing in the governing differential equations (6) will be thoroughly discussed in the next section.

III. CONTACT DYNAMICS

The contact model proposed in this paper conveys a mechanistic concept in calculating the contact forces as functions of the penetration depth between contact interfaces. This is the key improvement to the actuation model presented in [1], [2] in which a mathematics-based contact dynamics, i.e. curve fits to the experimental data obtained from felt compression, was utilized.

Recent experiments on a typical felt sample, shown in Fig. 1, reveals the existence of nonlinear hysteresis that is independent of speed of deformation [1]-[3]. It means that a viscoelastic relation to include hysteresis is not suitable for felt compression analysis. Thus, the focus should be on the friction between interacting fibers, assuming to be Coulomb type in which the frictional force is proportional to the applied normal force, independent of the contact area. The schematic of frictional fiber interaction at a typical contact point has been depicted in Fig. 4.

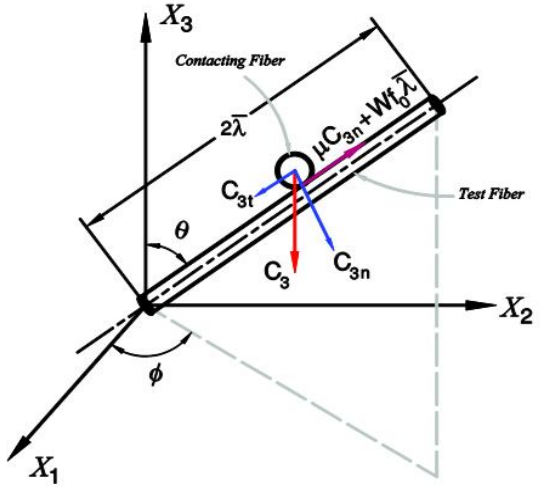


Fig.4. Contact forces developed in the fiber contact locations.

According to Coulomb's dry friction rule, the contacting fiber in Fig. 4 starts to slide on the test fiber if the tangential force exceeds the microscopic resisting force between the interacting surfaces that are in atomically close contact. That is [12],

$$C_{jt} \geq \mu C_{jn} + Wf_0\bar{\lambda} \Rightarrow C_j\cos(\theta) \geq \mu C_j\sin(\theta) + Wf_0\bar{\lambda} \quad (7)$$

where $CCjjjj$is the tangential force on the test fiber, $CCjjjj$is the normal force, $CCjj$ is the contact force in direction jj, $\mu\mu$ is the coefficient of friction, $\lambda\lambda$ is the mean free fiber length, and $WWff0$ is the withdrawal force per unit length of fiber in the absence of external loads on the fiber mass. The main source of withdrawal force comes from the fact that due to fiber interaction and friction, the fibers still have some residual bending energy in the absence of external loads on the fiber network.

In general, the macroscopic external load PP on the network must flow through fiber contact points. If $rrssss$ is the proportion of contact points that slide, the relation for macroscopic pressure can be written in case of loading as [2], [12]

$$P_{loading} = (1 - r_{sc})n_{\bar{\lambda}_j} C_{ns} + r_{sc}n_{\bar{\lambda}_j} C_s \Rightarrow P_{loading} = \sigma_{el} + r_{sc}n_{\bar{\lambda}_j} C_s \quad (8)$$

in which $CCss$ is the average contact force per sliding contact

point, $CCnnnn$is the the average contact force per non-sliding one, and $\sigma\sigma eeee$is the elastic stress

developed in the network during loading. $nn\lambda\lambda jj$is the number of contact points in the volume $VV\lambda\lambda jj$ with unit cross section area and the height $\lambda\lambda jj$ equal to the mean projection of the random fiber length on direction jj. For the unloading stage, it will be

$$P_{unloading} = (1 - r_{sc})n_{\bar{\lambda}_j} C_{ns} - r_{sc} n_{\bar{\lambda}_j} C_s \Rightarrow P_{unloading} = \sigma_{eu} - r_{sc} n_{\bar{\lambda}_j} C_s \quad (9)$$

in which $\sigma\sigma eeee$is the elastic stress developed in the network during unloading. It is obvious that all parameters in (8) and (9) are different in the cases of loading and unloading, i.e. $\sigma\sigma eeee \neq \sigma\sigma eeee$, and the effect of friction is not the same during loading and unloading. The proportion of contact points that slide, $rrssss$, can be estimated as [13] , [2]

$$r_{sc} = \int_0^{\theta_{cr}} \int_0^{\pi} \Omega(\phi, \theta) \sin(\theta)\, d\theta d\phi \quad (10)$$

where $\theta\theta cccc$ is the critical angle of sliding that can be acquired using (7) and $\Omega(\phi\phi,\theta\theta)$ is the fiber orientation distribution function for the fibers with polar and azimuthal angles $\phi\phi$ and $\theta\theta$ throughout the network.

The mean free fiber length, which is directly related to the number of fiber contacts, is the key parameter in the proposed micromechanical model of fiber networks. Masoudi et al. [2], [3] showed that the binomial distribution of fiber contacts presented by Neckář et al. [14] was the only scheme capable of reflecting the compression behavior of felt used in the contact interface of the model. Applying the approach, the pressure-volume fraction ($\upsilon\upsilon ff$) relation representing compression behavior of felt can be developed as follows [2], [14]:

$$P = K_p \left(\frac{\eta}{Q\gamma(1-\eta)}\right)^3 \left\{(1-\eta)\left[2 + \left(\frac{3}{2}\right)\frac{\eta}{1-\eta}\right] - \frac{\eta}{Q\gamma \upsilon_f}\right\} \quad (11)$$

which $\eta\eta$=1−ee−$QQQQ\upsilon\upsilon ff$ and $KKpp$ is an uncertainty parameter, containing fiber modulus of elasticity, that accounts for all assumptions, approximations, and averaging errors that appear in the mechanistic model. The volume fraction of the network represents the bulk deformation and QQ=2 for spatial random fiber networks. Considering the experimental data from the felt compression for the felt underneath the key (see Fig. 2), the elastic portion of loading ($\sigma\sigma eeee$) and unloading ($\sigma\sigma eeee$) curves can be represented by (11).

It is important to note that (11) is a physics-based relation with parameters linked to the geometrical and physical properties of the fiber network. The inelastic part, which accounts for the loss due to friction between fibers, will be estimated using the second part of (8) and (9). A detailed procedure to obtain $PPllllllllllll$ and $PPuuuuuuuuuuuuuuuuuu$has been described in [2], [3]. To model the hysteretic behavior and consider partial loading and unloading during interaction of contact interfaces, the following mathematical relation is applied:

$$F_n(\varepsilon_p, \upsilon_n) = \begin{cases} F_L(\varepsilon_p), & \text{if } \upsilon_n > 0 \\ F_L(\varepsilon_p) + \delta_{LU}(\varepsilon_p)\tanh(\alpha\, \upsilon_n), & \text{if } \upsilon_n < 0 \end{cases} \quad (12)$$

where $FFnn$ is the normal contact force, $\varepsilon\varepsilon pp$ is the penetration depth (directly related to volume fraction $\upsilon\upsilon ff$), $\delta\delta LLLL(\varepsilon\varepsilon pp)$=$FFLL(\varepsilon\varepsilon pp)$−$FFUU(\varepsilon\varepsilon pp)$ is the difference between the loading and unloading curve fits at each penetration depth, $\alpha\alpha$ is a constant that controls the transition speed between loading and unloading states, and $\upsilon\upsilon nn$ is the normal speed between the two surfaces at the contact point, which also influences the transition. The relation defined in (12) confines the partial loading and unloading curves to lie within the experimental hysteresis loop used to obtain the curve fits, i.e. $FF(\varepsilon\varepsilon pp) \leq FFnn(\varepsilon\varepsilon pp) \leq FFLL(\varepsilon\varepsilon pp)$.

IV. SIMULATION RESULTS AND DISCUSSION

As the vibration response of the actuator is characterized mainly by its behavior during contact with the stop, the only significant input requirement is to ensure that a realistic impact speed is achieved, and that sufficient force is provided to hold the key down on the felt after impact. Consequently, a simple ideal ramp function from zero to 3N.m in the first 0.06s, with subsequent constant holding torque of 3N.m, is used for input torque in the simulation. To extract geometrical and mass information for the hub and arms, a 3D-model for each body was constructed in SolidWorks software [15]. The estimates of location of center of mass and the mass moment of inertia about center of the hub were extracted from the CAD model. Two types of arms have been considered in replicating the desired finger-key contact force. Numerical values of the actuator mechanism parameters including mass and structural parameters of the hub, wooden arm, and aluminum arm are listed in Table 1.

Table 1: Geometry and material properties of the key actuator components.

Part Description	Unit	Aluminum arm	Wood arm
Hub effective radius	m	61.08E-03	68.48E-03
Effective length of the beam	m	38.85 E-03	33.05E-03
Mass density	Kg/m^3	2.54E+03	7.74 E+02
Cross section area	m^2	81.44E-06	22.39E-06
Beam modulus of elasticity	Pa	6.83E+10	10.0E+09
Second moment of area	m^4	283.25E-12	5.93E-12
Moment of inertia of the hub	kg.m^2	51.35E-06	51.35E-06
Tip mass	Kg	1.57E-03	1.29E-03
Eccentricity	m	3.39E-03	5.00E-03

Using the symbolic capabilities of Maple software [16], we obtained the local mass, stiffness, and generalized force matrices, including effect of gravity, for each element. The associated global matrices are obtained by exporting the obtained local matrices into Matlab [17] and assembling them in the global locations as described in [1]. In this work,

a stiff solver, ODE15s, was applied and the results for rotation angle and tip deflection of the wood arm are shown in Fig. 5.

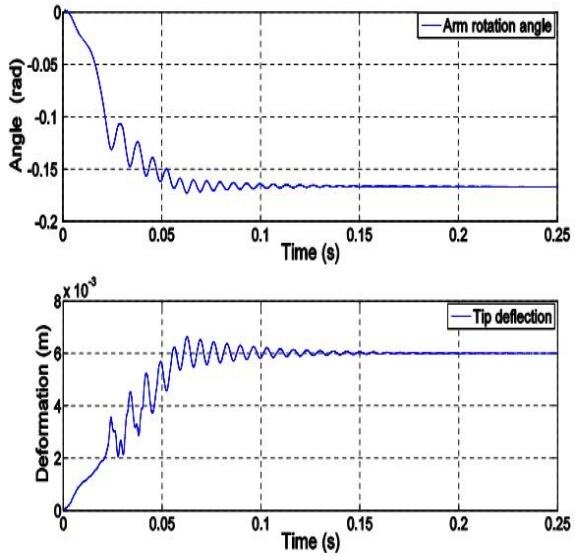


Fig.5. Simulated rotation angle and tip deflection of the wood arm in case of no damping.

For the aluminum arm, the rotation angle and tip deflection would be as shown in Fig. 6.

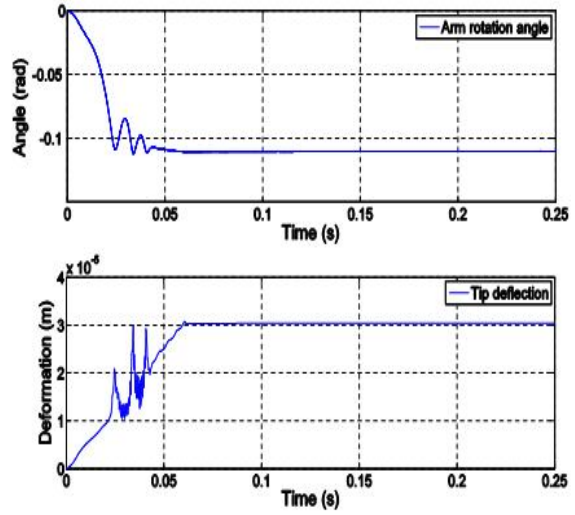


Fig.6. Simulated rotation angle and tip deflection of the aluminum arm in case of no damping.

As can be expected, the vibrations for the wooden arm are more severe in terms of magnitude and duration compared to the stiffer aluminum arm. These vibrations can affect the dynamic behavior of the key, and thereby also the whole piano action response. Thus, comparing the oscillations with the experiment in the future can help us in developing a more realistic actuation system representing the input to the piano action mechanism. Finger-key contact force as would be measured by a force sensor between input arm and key can be calculated for simulations by adding the reaction force generated by the piano action to the interaction force between key and felt.

Simulation results for the two types of finger arm are shown in Fig. 7. The similarities between the simulated force profile for the aluminum arm and that generated by the actual motor aluminum arm presented in [1], [2] confirm the validity of the assumptions and simplifications used in modeling the actuator system. It is worthwhile to note that the difference between the first peaks in the force profiles is mainly due to the different reaction from the piano action compared to the approximate reaction force used in simulations; however this does not affect significantly the results of vibration response significantly. Furthermore, the torque applied on the hub by the motor is somewhat different from the ideal torque profile used for simulations.

A rigid actuator such as the one with the aluminum arm produces larger amplitude vibrations with longer duration than does a pianist's finger. Adding compliance to the arm has been proposed to improve this situation, for instance through the use of a flexible wooden arm, but, as can be seen in the simulation results of Fig. 6, this is not sufficient to eliminate the problem. Additionally, some source of damping must be incorporated into the actuation system, if the input response is to better match that of the pianist.

It is important to note that since the micromechanical contact model represents the real hysteresis curves corresponding to hammer-string contact point, the results are very similar to the ones presented in [1], [2], which is based on a math-based contact model, i.e. curve-fitting to the experimental felt compression data. The main difference is a longer simulation time due to extensive computational effort in estimating force-penetration relations for the physics-based contact model during the simulation.

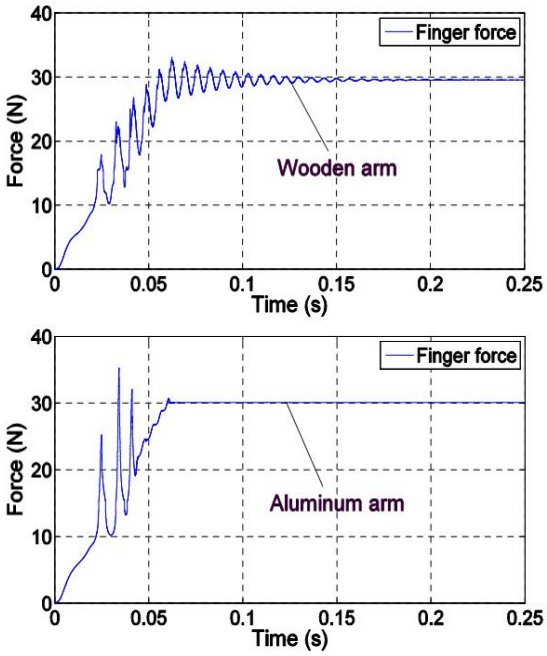


Fig.7. Simulated finger force generated between key and tip mass for wooden and aluminum arms in case of no damping.

Of course, although these simulations took longer than those using the mathematical contact model, this

technique is still encouraging for the simulation of the dynamic system.

CONCLUSION

Dynamic modeling of a device to achieve a desired finger-key contact force profile that realistically replicates that of a real pianist's finger was presented. The proposed actuation system consists of a flexible arm which is attached to a DC brushless rotary motor through a hub. The compliant arm behaves as a cantilever beam to which an eccentric tip mass has been attached at its free end. During the piano key stroke, the contact force input from the tip causes the key to

rotate and impact the ground through an interface lined with stiff felt to suppress vibrations and noise. Euler-Bernoulli beam theory in conjunction with Lagrange's method is utilized to obtain the governing equations of motion for the system. The flexible cantilever beam, representing a distributed parameter system, is discretized using finite element method. To include contact dynamics at the stop, the nonlinear hysteretic behavior of felt under compression is modeled mechanistically in such a way that smooth transitions between loading and unloading stages are produced, thus ensuring accurate response under dynamic conditions, and particularly with partial loading and unloading states that occur during the contact period.

A micromechanical model for nonlinear compression hysteresis of random fiber networks was developed and examined on felt, a fiber assembly with random structure, exhibiting velocity-independent hysteretic behavior in compressive loading schemes. A binomial distribution of fiber contacts, together with the Coulomb friction criterion for fiber sliding, have been used to construct the nonlinear hysteretic behavior of the network. The efficacy of the proposed contact model was examined in vibration analysis of the flexible hub-beam system including felt-lined contact interfaces.

REFERENCES

[1] R. Masoudi, S. Birkett, and A. Salehian, "Dynamic simulation and vibration analysis of a mechanical piano key actuator," ASME 2011 International Design Engineering Technical Conferences and Computers and Information in Engineering Conference, American Society of Mechanical Engineers, 2011.

[2] R. Masoudi, "Micromechanics of Fiber Networks Including Nonlinear Hysteresis and its Application to Multibody Dynamic Modeling of Piano Mechanisms," PhD Thesis, University of Waterloo, Canada, 2012.

[3] R. Masoudi and J. McPhee, "A novel micromechanical model of nonlinear compression hysteresis in compliant interfaces of multibody systems," Multibody System Dynamics, pp. 1-19, 2015.

[4] G. Gilardi and I. Sharf, "Literature survey of contact dynamics modelling," Mechanism and Machine Theory, vol. 37, no. 10, pp. 1213-1239, 2002.

[5] P. Flores, M. Machado, and M.T. Silva, "On the continuous contact force models for soft materials in multibody dynamics," Multibody System Dynamics, vol. 25, no. 3, pp. 357-375, 2011.

[6] G. P. Cai, J. Z. Hong, and S. X. Yang, "Dynamic analysis of a flexible hub-beam system with tip mass," Mechanics Research Communications, vol. 32, no. 2, pp. 173-190, 2005.

[7] B. V. Chapnik, G. R. Heppler, and J. D. Aplevich. Modeling impact on a one-link flexible robotic arm. IEEE Transactions on Robotics and Automation, vol. 7, no. 4, pp. 479-488, 1991.

[8] A. S. Yigit, A. G. Ulsoy, and R. A. Scott, "Dynamics of a radially rotating beam with impact part 1: theoretical and computational model," Journal of Vibration and Acoustics, vol. 112, no. 1, pp. 65-70, 1990.

[9] A. S. Yigit, A. G. Ulsoy, and R. A. Scott, "Dynamics of a radially rotating beam with impact, part 2: experimental and simulation results," Journal of Vibration and Acoustics, vol. 112, no. 1, pp. 71-77, 1990.

[10] A. S. Yigit, A. G. Ulsoy, and R. A. Scott, "Spring-dashpot models for the dynamics of a radially rotating beam with impact," Journal of Sound and Vibration, vol. 142, no. 3, pp. 515-525, 1990.

[11] M. Hirschkorn, "Dynamic Model of a Piano Action Mechanism," MSc Thesis, University of Waterloo, Canada, 2004.

[12] G. A. Carnaby and N. Pan, "Theory of the compression hysteresis of fibrous assemblies," Textile Research Journal, vol. 59, pp. 275-284, 1989.

[13] T. Komori and K. Makishima, "Numbers of fiber-to-fiber contacts in general fiber assemblies," Textile Research Journal, vol. 47, pp. 13-17, 1977.

[14] B. Neckář and S. Ibrahim, "A contribution to van Wyk's theory of contacts between fibers," In Advanced Flexible Materials and Structures: Engineering with Fibers, The Fiber Society 2003 Spring Symposium, Loughborough University, UK, 2003.

[15] SolidWorks Office Premium, SolidWorks 2007 Online User's Guide-SP0.0, Solid-Works Corporation, Concord, Massachusetts, USA, 2007.

[16] Maplesoft, Maple 18 User Manual, Maplesoft, a division of Waterloo Maple Inc., Waterloo, ON, Canada, 2014.

[17] Matlab, Version 8.5.0.197613 (R2015a), The MathWorks Inc., Natick, Massachusetts, 2015.

★★★